

# Parametrization and validation of a force field for liquid-crystal forming molecules

D. L. Cheung,<sup>1,2</sup> S. J. Clark,<sup>2</sup> and M. R. Wilson<sup>1</sup>

<sup>1</sup>*Department of Chemistry, University of Durham, South Road, Durham DH1 3LE, United Kingdom*

<sup>2</sup>*Department of Physics, University of Durham, South Road, Durham DH1 3LE, United Kingdom*

(Received 23 January 2002; published 21 May 2002)

First principles density functional calculations have been carried out to determine the structures and conformational energies of a series of liquid-crystal fragment molecules. The calculations have been used to derive a molecular mechanics force field that describes a subset of commonly occurring liquid-crystal molecules. The force field has been used to carry out molecular dynamics simulations of the bulk phase for these fragment molecules. Computed densities and heats of vaporization are in good agreement with experimental data. These results should be useful in future molecular dynamics simulations of liquid-crystal systems.

DOI: 10.1103/PhysRevE.65.051709

PACS number(s): 61.30.Cz, 31.15.Ar, 02.70.Ns

## I. INTRODUCTION

Classical Monte Carlo and molecular dynamics computer simulations are now regarded as powerful tools in the study of soft condensed matter systems, including polymers, liquid crystals, and complex fluids. However, the ability of these simulations to predict material properties is influenced strongly by the accuracy of the model used. For liquid crystals simple hard [1,2] and soft [3–6] single site models have been successful in modeling nematics and a range of smectic phases. Single site models, such as spherocylinders or Gay-Berne units do not allow for molecular shape to change during the course of a simulation. However, liquid crystals are inherently flexible and this flexibility has a significant influence on both phase behavior and material properties [7,8] and, therefore, must be included in any realistic model of a material. Atomistic models provide a convenient way of incorporating molecular flexibility into simulations of liquid crystals. In comparison to simple single site models, atomistic work is extremely expensive in terms of computer time. However, recent increases in computer power and the development of parallel simulation methods [9] have led to a number of atomistic studies [10–18].

Many of the the early atomistic simulations of liquid crystals suffered from a poor description of both the intramolecular and intermolecular interactions. Force fields to represent atomistic systems typically require terms to describe bond stretching, bond angle bending, and internal rotations in addition to nonbonded interactions. Traditionally, these have been derived from a variety of sources including experimental data, such as spectroscopy or crystallography. *Ab initio* calculations can also be used. In principle, such calculations can achieve a high level of accuracy and can probe intramolecular interactions that are experimentally difficult.

In this work, we use state-of-the-art density functional theory calculations to construct atomistic potentials to describe many of the key structural motifs in common calamitic liquid crystals that are used in display applications. In particular, we have fitted potential functions for biphenyls, phenylcyclohexane cores, alkyl chains, lateral fluorine substituents, and cyano groups. These include functions for bond stretching, bond angle bending and, most crucially, internal rotations. This paper is organized as follows. The choice of

functional form is discussed briefly in Sec. II and the computational method is outlined in Sec. III. The results from the density functional calculations and bulk simulations using the derived force field are presented in Sec. IV. Finally, we summarize these results and discuss briefly the avenues for future work in Sec. V.

## II. FORM OF THE FORCE FIELD

The choice of functional form for a force field is influenced strongly by its intended use. For instance, there is a large difference between the preferred functional form for a force field designed for simulation of bulk phases, such as the AMBER force field [19], and that of a force field designed for the determination of gas phase structures, such as MM4 [20–23]. For simulation of bulk phases at room temperature it is rarely necessary to use anharmonic terms to describe variations in bond lengths and angles. Consequently, for this work, we employ a force field of the AMBER form [19], with harmonic terms for bond stretching and bond angle bending, and a Lennard-Jones 12-6 potential [24] for interatomic repulsion and attraction instead of computationally more expensive forms used in other force fields. So for this force field, which is intended for the simulations of condensed liquid-crystal phases, the AMBER form [19] is the most appropriate.

Thus our force field has the functional form

$$E_{ff} = E_{stretch} + E_{bends} + E_{tor} + E_{vdw} + E_{elec}, \quad (1)$$

where the terms for bond stretching, bond angle bending, torsional rotation, van der Waals, and electrostatic energies are as follows:

$$E_{stretch} = \sum_{bonds} \frac{1}{2} k_l (l - l_{eq})^2, \quad (2)$$

$$E_{bends} = \sum_{angles} \frac{1}{2} k_\theta (\theta - \theta_{eq})^2, \quad (3)$$

$$E_{tor} = \sum_{dih} \sum_n \frac{1}{2} k_\tau [1 + \cos(n\tau + \delta_n)], \quad (4)$$

$$E_{vdw} = \sum_{i,j} 4\epsilon_{ij} \left[ \left( \frac{\sigma_{ij}}{r_{ij}} \right)^{12} - \left( \frac{\sigma_{ij}}{r_{ij}} \right)^6 \right], \quad (5)$$

$$E_{elec} = \sum_{i,j} \frac{1}{4\pi\epsilon_0} \frac{q_i q_j}{r_{ij}}. \quad (6)$$

Here  $k_l$ ,  $k_\theta$ , and  $k_\tau$  are the force constants for bond bending, bond angle bending, and torsional rotations, respectively,  $l_{eq}$  and  $\theta_{eq}$  are the equilibrium bond lengths and angles,  $\epsilon_{ij}$  and  $\sigma_{ij}$  are the van der Waals well depth and collision parameters (distance at which  $E_{vdw}=0$ ), and  $q_i$  are the atomic charges.  $l$ ,  $\theta$ , and  $\tau$  are the bond lengths, bond angles, and torsional angles, respectively, and the sums in Eqs. (5) and (6) run over all pairs of atoms without a common bond or bond angle. In some fluorinated molecules, particularly those with lateral fluorine substituents, hydrogen and fluorine atoms can come into close proximity to each other, well inside the van der Waals radius. This leads to strong repulsion between them, which complicates the fitting of torsional parameters. To counter this, we model the van der Waals interaction for molecules using an exponential-6-type potential [25]

$$E_{vdw}^{HF} = \epsilon_{ij} \left[ \frac{6}{\alpha-6} \exp \left[ \alpha \left( 1 - \frac{r}{6\sqrt{2}\sigma_{ij}} \right) \right] - \frac{2\alpha}{\alpha-6} \left( \frac{\sigma_{ij}}{r} \right)^6 \right], \quad (7)$$

where  $\alpha$  is an adjustable parameter. In this study we use  $\alpha = 12$ , which gives the same long-range behavior as the Lennard-Jones potential [25].

In the nonbonded (van der Waals and electrostatic) terms, the sums exclude nonbonded interactions between the atoms that have a common bond (1-2) or bond angle (1-3). In common with the merged AMBER/optimized parameters for liquid simulation (OPLS) force field, we scaled 1-4 (atoms sharing a common dihedral) van der Waals interactions by  $\frac{1}{2}$  and the 1-4 electrostatic interactions by  $\frac{1}{8}$ . The Fourier series for the torsional energy is expanded in enough terms to reduce the squared difference between the *ab initio* energies and the fitted energies to below 0.0019 eV<sup>2</sup>.

### III. COMPUTATIONAL METHOD

#### A. *Ab initio* calculations

Structural and conformational energies were computed within the *ab initio* density functional formalism [26,27] using a plane wave basis set for the valence electrons. The CASTEP program [28,29] was used for these calculations. To reduce the computational cost, the electron-ion interaction is described using ultrasoft pseudopotentials of the Vanderbilt form [30] and the PW91 generalized gradient approximation [31] is used for the evaluation of the exchange-correlation interactions.

In this method, a molecule is placed in the center of a periodically repeating supercell, and a plane wave basis set is employed, which was expanded to a kinetic energy cutoff of 400 eV, giving energy differences accurate to within 0.001 eV/atom. To avoid interactions between molecules in neigh-

boring cells, a supercell is constructed, which is large enough to isolate the molecule from its periodic images. Only a single  $k$  point is required as the electronic bands are dispersionless for isolated molecules.

The use of a plane wave basis set combined with pseudopotentials gives several advantages over the more commonly used localized basis sets used in quantum chemical calculations for the molecules. These include (i) the same basis set can be used for all atomic species, (ii) basis set completeness can be guaranteed, and (iii) force calculations do not require corrections.

To find the optimized molecular geometry an initial structure is constructed first by using the modeling package Cerius<sup>2</sup> [32]. The Hellman-Feynman [33] theorem is then used to calculate the force on each atom and then the atoms are moved under the influence of these forces until the force falls below a set tolerance. The optimization is converged when the residual force on the atoms falls below 0.05 eV Å<sup>-1</sup>. For the calculation of torsional angle potentials, the chosen dihedral is held fixed, while the remaining degrees of freedom are relaxed.

#### B. Fitting of force field parameters

Force field parameters were found by fitting to potential energy surfaces of common liquid crystal components. These included biphenyls, with terminal cyano substitution and lateral fluorine substitutions, as well as other core components. Potentials for ring-tail torsions were calculated using propylbenzene. The force field parametrization is based on the atom types shown in Table I, which in turn are based on the notation used for the AMBER force field [19].

Force field parameters for bond stretching and bond angle bending were found by fitting the *ab initio* potentials to the bond stretching and bond angle bending potentials in Eqs. (2) and (3). We can also derive the force field parameters from the forces on the atoms

$$F_l = -k_l(l - l_{eq}). \quad (8)$$

For small deviations from equilibrium, the potentials are harmonic, as can be seen in Fig. 1.

The van der Waals parameters are not easily found by density functional methods. In this work they are taken from the OPLS parameter set [34–36] of Jorgensen *et al.*, as were most of the atomic charges. The OPLS parameters have been shown to reproduce experimental values for various thermodynamics quantities, including densities and heats of vaporization with an average error of 2–3% [34]. Partial charges for aromatic carbon and hydrogen atoms were found by least-squares fitting to the electrostatic quadrupole moment of benzene, yielding values of  $-0.122e$  and  $+0.122e$ , respectively. Charges for other atom types were taken from the OPLS parameter set.

Torsional force constants  $k_\tau$  were found by a least-squares fit to the *ab initio* potential using the torsional force constants as free parameters. The fitting procedure was as follows: (i) start with approximate values for  $k_\tau$ , (ii) minimize the energy of the molecule at each *ab initio* data point, and (iii) calculate the sum of squared differences between the

TABLE I. Described here are the force field atom types and the definitions used in this paper.

Atom type	Description
C <sub>A</sub>	Aromatic carbon
C <sub>P</sub>	Aromatic carbon (joining aromatic rings)
H <sub>A</sub>	Aromatic hydrogen
C <sub>Z</sub>	Carbon in cyano group
N <sub>Z</sub>	Nitrogen in cyano group
C <sub>n</sub>	Aliphatic carbon [ <i>n</i> indicates number of attached hydrogens ( <i>n</i> =0,1,2,3,4)]
HC	Aliphatic hydrogen
F	Fluorine
OH	Alcohol oxygen
HO	Alcohol hydrogen

*ab initio* data and the data obtained from the energy minimizations. Although time consuming, this method ensures that all other contributions to the molecule's torsional potential (including van der Waals and electrostatic contributions) are accounted for in the fit. All minimizations were performed using Powell's method [37]. By convention, the phase angles  $\delta_n$  were set to  $0^\circ$  for odd *n* and  $180^\circ$  for even *n*, so that the terms with positive  $k_{\tau i}$  have minima at  $180^\circ$ .

### C. Molecular dynamics simulations

The simulations were performed using the DL-POLY program [38] (versions 2.11 and 2.12). The equations of motion were integrated using the leapfrog algorithm with a time step of 2 fs. Bond lengths were constrained using the SHAKE procedure [39]. The temperature and pressure were controlled using a Nosé-Hoover thermostat and Hoover barostat [40], respectively, with relaxation times of 1 ps and 4 ps. Electrostatic interactions were handled using an Ewald sum [41]

with an Ewald convergence parameter of  $0.48 \text{ \AA}^{-1}$  and six wave vectors in the *x*, *y*, and *z* directions in accordance with previous work [42]. A 9- $\text{\AA}$  cutoff was imposed on the van der Waals interactions along with long-range corrections for the energy and virial. A Verlet neighbor list [41] was used to speed up calculation of nonbonded forces.

The simulations were started from a cubic lattice of 216 molecules at a gas phase density (about  $1 \text{ kg m}^{-3}$ ). They were then compressed under a nominal pressure of 10 kbars until a liquid state density ( $500\text{--}1000 \text{ kg m}^{-3}$ ) was reached. This was performed at 100 K, which ensured that a rapid compression took place. The systems were then heated up to the simulation temperatures (the melting points for biphenyl, 4-cyanobiphenyl, and 2-fluorobiphenyl, the boiling point in the case of butane, and 298 K for the others) and equilibrated for up to 1 ns (500 000 time steps) until the system temperature, volume, and configurational energy showed no sign of systematic drift. Statistics were then gathered over a 1-ns production run.

## IV. RESULTS

### A. Force field parameters

Shown in Fig. 1 are the energy and force plotted for stretching aromatic C-H and cyano C-N bonds. Both the po-

TABLE II. The bond stretching force constants ( $k_l$ ) and equilibrium bond lengths ( $l_{eq}$ ) are given here for a range of bonds found in liquid-crystal fragments.

Bond	$k_l$ ( $\text{eV \AA}^{-2}$ )	$l_{eq}$ ( $\text{\AA}$ )
C <sub>A</sub> -H <sub>A</sub>	33.96	1.08
C <sub>A</sub> -C <sub>A</sub>	44.32	1.38
C <sub>A</sub> -C <sub>P</sub>	44.32	1.38
C <sub>P</sub> -C <sub>P</sub>	27.28	1.47
C <sub>A</sub> -C <sub>Z</sub>	31.52	1.31
C <sub>Z</sub> -N <sub>Z</sub>	115.11	1.17
C <sub>A</sub> -C <sub>n</sub>	24.47	1.50
C <sub>n</sub> -C <sub>n</sub>	22.97	1.51
C <sub>n</sub> -HC	31.65	1.09
C <sub>A</sub> -F	35.08	1.36
C <sub>A</sub> -OH	38.89	1.36
OH-HO	52.06	0.97

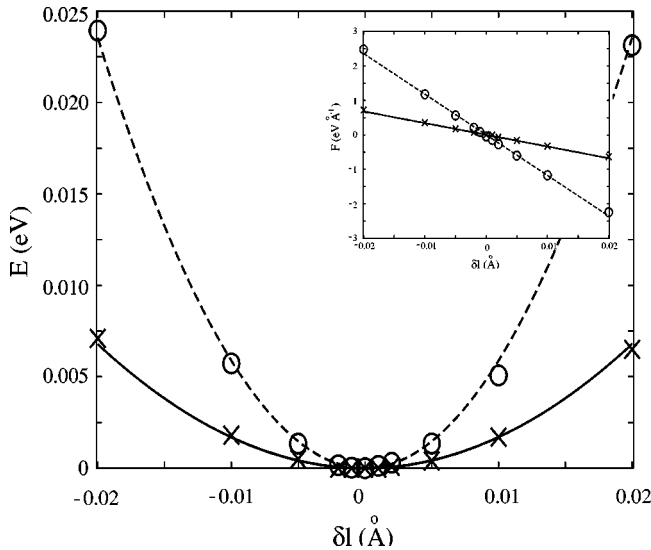


FIG. 1. Bond stretching potentials for C-H bond in biphenyl [the *ab initio* data ( $\times$ ) and the fitted data ( $-$ )] and the C<sub>Z</sub>-N<sub>Z</sub> bond in 4-cyanobiphenyl [the *ab initio* data ( $\circ$ ) and the fitted data ( $--$ )]. Inset shows the variation of force with change in bond length. Here  $\delta l = l - l_{eq}$ .

TABLE III. Bond angle bending force constants ( $k_\theta$ ) and equilibrium bond angles  $\theta_{eq}$ .

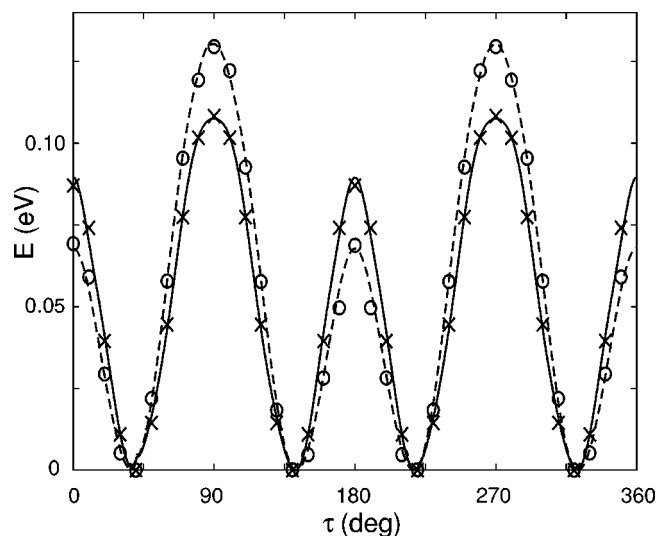
Angle	$k_\theta$ ( $\times 10^{-5}$ eV/deg <sup>2</sup> )	$\theta_{eq}$ ( $^\circ$ )
C <sub>A</sub> -C <sub>A</sub> -H <sub>A</sub>	98.46	120
C <sub>A</sub> -C <sub>A</sub> -C <sub>A</sub>	84.94	120
C <sub>A</sub> -C <sub>P</sub> -C <sub>P</sub>	95.32	120
C <sub>A</sub> -C <sub>A</sub> -C <sub>Z</sub>	134.38	120
C <sub>A</sub> -C <sub>Z</sub> -N <sub>Z</sub>	71.10	180
C <sub>n</sub> -C <sub>n</sub> -C <sub>n</sub>	244.76	113
C <sub>n</sub> -C <sub>n</sub> -HC	116.98	112
HC-C <sub>n</sub> -HC	147.25	107
C <sub>A</sub> -C <sub>A</sub> -F	101.90	120
C <sub>A</sub> -C <sub>A</sub> -OH	98.27	120
C <sub>A</sub> -OH-HO	70.93	109

tentials show a quadratic dependence on the change in bond length as expected from Eq. (2) and the forces vary linearly with the change in bond length as expected from Eq. (8). The force field parameters for bond stretching are listed in Table II and those for bond angle bending are shown in Table III. Table IV provides a comparison of our bond stretching force constants for the aliphatic C-C and C-H bond stretches compared with those from the OPLS [35], MM3 [43], MMFF94 [44], and AMBER [19] force fields. Our values show reasonable agreement, notably with the OPLS that employs the same harmonic form, and MMFF94 values. This is indicative of the quality of our *ab initio* calculations; we obtain comparable results from the density functional calculations as those from high level (MP2) quantum chemical calculations.

While bond stretching and bending parameters can be transferred across a wide range of molecules, torsional parameters can be less transferable. This can be seen especially in conjugated systems where terminal polar substituents have a large effect on the torsional potential [45], which is not accounted for either through the electrostatic or through the van der Waals interactions. An example of this can be seen by comparing the torsional potentials for biphenyl and 4-cyanobiphenyl shown in Fig. 2. Here we can see a marked difference in the torsional potentials, caused by charge transfer towards the polar cyano group. This effects the bonding and structure in the molecule, changing the trade-off between steric repulsion and conjugation. The classical nonbonded

TABLE IV. Comparison of bond stretching force constants for aliphatic C-C and C-H bonds, between this work and other force fields.

Force field	C <sub>n</sub> -C <sub>n</sub> bond		References
	$k_l$ (eV Å <sup>-2</sup> )	$k_l$ (eV Å <sup>-2</sup> )	
This work	22.97	31.65	
OPLS	23.22	29.40	[35]
MM3	28.03	29.59	[43]
MMFF94	23.72	32.15	[44]
AMBER	26.90	28.71	[35]

FIG. 2. Torsional angle potentials for biphenyl [the *ab initio* potential ( $\times$ ) and the fitted potential ( $-$ )] and 4-cyanobiphenyl [the *ab initio* data ( $\circ$ ) and the fitted data ( $--$ )].

torsional potentials for these molecules are shown in Fig. 3. As the nonbonded potentials are identical, different torsional parameters are required to reproduce the *ab initio* potentials.

The torsional barrier of biphenyl has been the subject of a number of previous studies, both theoretical [22,46–48] and experimental [49–52]. As can be seen from Fig. 2 we have been able to reproduce the torsional potentials accurately through the fitted potentials. The rotational barrier at  $0^\circ$  for biphenyl is found to be 0.089 eV for the fitted potential and 0.087 eV from the *ab initio* data. The rotational barrier at  $90^\circ$  is 0.108 eV from the fitted potential and 0.108 eV from the *ab initio* data. A previous study using the density functional theory (DFT) with the 6-31G(d) basis set [47] found the energy barriers to be 0.087 and 0.104 eV. However, the present results benefit from a more complete basis set than the earlier study. The barrier heights have been calculated

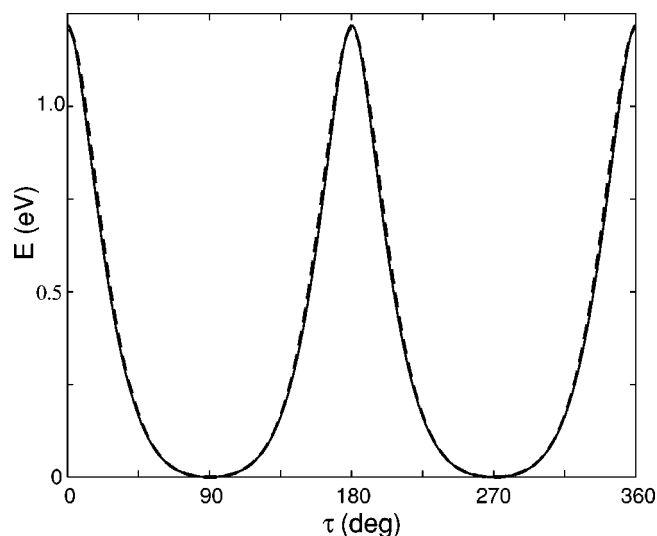
FIG. 3. Variation of nonbonded energy against torsional angle for biphenyl ( $-$ ) and 4-cyanobiphenyl ( $--$ ).

TABLE V. Comparison of rotational barrier heights for biphenyl between this work and previous studies (barrier heights in eV).

Method	References	$\Delta E_0$	$\Delta E_{90}$
PW-DFT (GGA)	This work	0.087	0.108
Fitted potential	this work	0.089	0.108
MM4	[22]	0.107	0.080
HF/6-31G*/MP2/6-31G*	[46]	0.141	0.063
MP2/cc-PVQZ//MP2/6-31G*	[46]	0.098	0.092
MP2/6-31G(d)	[47]	0.169	0.091
B3-LYP/6-31G(d)	[47]	0.087	0.104
B3LYP/cc-pVTZ	[48]	0.083	0.092
Electron diffraction	[49,50]	0.061	0.069
Raman scattering	[51]	0.061	0.061
NMR	[52]	0.079	0.226

using a number of wave function based methods [46,48], which give barrier heights of about 0.98–0.141 eV for the 0° barrier and 0.63–0.92 eV for the 90° barrier. Again these values have been obtained using a smaller basis set than in this work. Experimentally  $E_0$  has been found to be between 0.061 and 0.079 eV and  $E_{90}$  between 0.061 and 0.226 eV. These results are summarized in Table V, along with results from the MM4 force field [22]. Our 0° barrier is lower than that given by the wave function methods and consistent with other DFT calculations and also with experiment as expected. The 90° barrier is somewhat larger than those calculated by wave function methods as well as the electron diffraction and Raman scattering results, although it is substantially lower than that given by nuclear magnetic resonance (NMR) measurements. The NMR measurements, however, were performed on biphenyl in a liquid crystalline solvent, while the other experimental and computational results are for molecules in the gas phase. In agreement with experimental measurements, we have  $E_{90} > E_0$ .

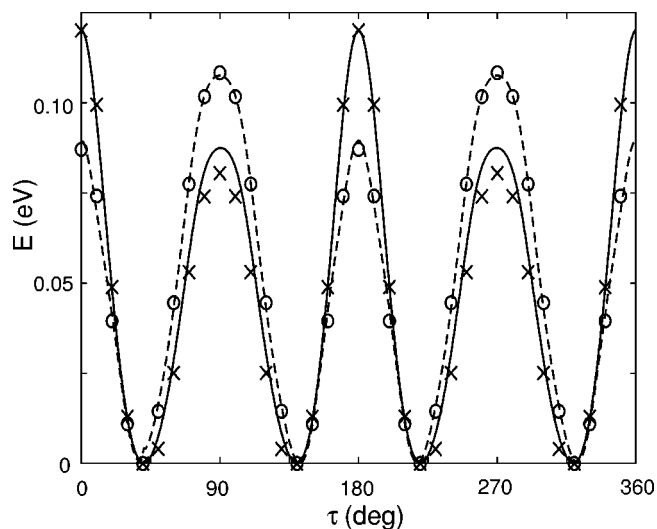


FIG. 4. Torsional angle potentials for 2-fluorobiphenyl [the *ab initio* potential (×) and the fitted potential (—)] and for biphenyl [the *ab initio* potential (○) and the fitted potential (---)].

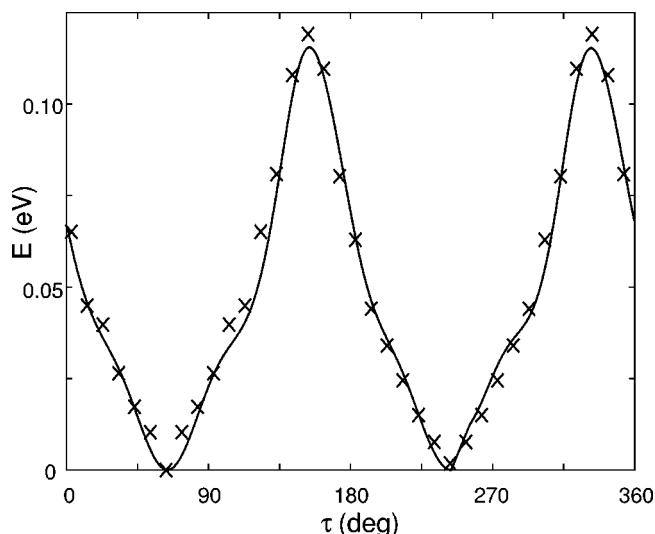


FIG. 5. Torsional angle potential for phenylcyclohexane [the *ab initio* potential (×) and the fitted potential (—)].

For 4-cyanobiphenyl the barrier heights at 0° and 90° are 0.073 eV and 0.130 eV, respectively, from the fitted potential and 0.069 eV and 0.130 eV from the *ab initio* data. Previous *ab initio* calculations at the Hartree-Fock (HF)/6-31G level found the barriers to be 0.212 eV and 0.067 eV [53]. The 0° and 90° barrier heights have been determined by NMR [54] to be 0.079 and 0.241 eV, respectively. Again the NMR results are for cyanobiphenyl dissolved in a liquid-crystal solvent. In agreement with experiment and in contrast to the Hartree-Fock results we have  $E_0 < E_{90}$  that underlines the greater accuracy of our method compared to earlier calculations.

Lateral polar substituents are commonly used in liquid crystals to produce materials with a negative dielectric anisotropy. However, the decrease in the length to width ratio caused by these substituents causes a decrease in the clearing temperature and the mesophase stability. They also have a large effect on the torsional potentials of conjugated systems.

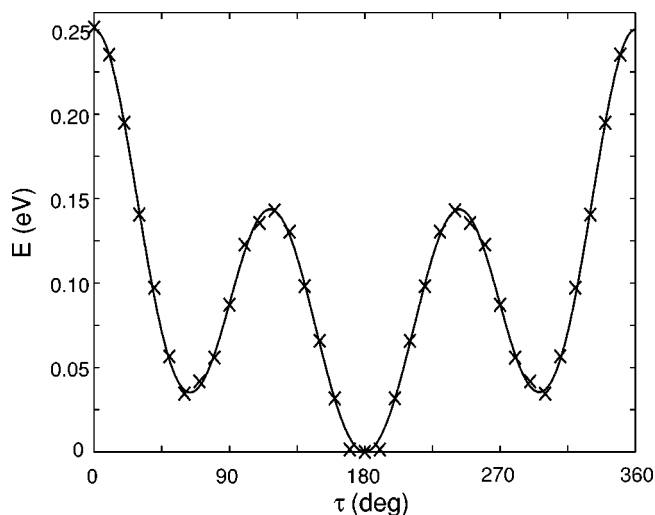


FIG. 6. Torsional angle potential for butane [the *ab initio* potential (×) and the fitted potential (—)].

TABLE VI. Comparison of rotational barrier energies for butane between this work and previous studies (barrier heights in eV).

Method	References	$\Delta E_{t-g}$	$E_{120^\circ}$	$E_{0^\circ}$
PW-DFT (GGA)	This work	0.035	0.142	0.251
Fitted potential	This work	0.034	0.140	0.251
HF/6-31G**//HF/6-31G*	[60]	0.041	0.159	0.268
MP2/6-31G**//MP2/6-31G*	[60]	0.029	0.157	0.263
MP4(SDTQ)/6-31G**//MP2/6-31G*	[60]	0.031	0.154	0.257
QCISD(T)/6-31G**//MP2/6-31G*	[60]	0.031	0.152	0.255
BLYP/6-31G**//BLYP/6-31G*	[60]	0.037	0.150	0.245
MM4	[22]	0.029	0.147	0.214
Raman scattering	[57]	0.039	0.157	0.196
Thermodynamic	[56]	0.035	0.156	
IR in solid Ne	[58]	0.032		
Electron diffraction	[59]	0.033		

In addition to changing the conjugation of the system, they also create highly dipolar regions that give rise to strong electrostatic interactions. For liquid-crystal molecules, the most common lateral substituent is fluorine, because it has the smallest effect on the phase stability due to its small size. Figure 4 shows both the *ab initio* and fitted potentials for 2-fluorobiphenyl along with that of biphenyl for comparison. Again there is good agreement between the fitted and *ab initio* potentials. The *ab initio* energy barriers at  $0^\circ$  and  $90^\circ$  are 0.119 eV and 0.080 eV, respectively, while the fitted barriers are 0.124 eV and 0.085 eV. There has been little previous work on this torsional potential. Calculations at the relativistic Hartree-Fock/6-31G level have found the  $0^\circ$  barrier to be 0.147 eV and the  $90^\circ$  barrier to be 0.061 eV [42]. However, as above, our calculations can be expected to be somewhat more accurate. The torsional potential has also been calculated using the MM3 force field that gives the  $0^\circ$  barrier to be 0.383 eV and the  $90^\circ$  barrier to be 0.012 eV.

Another common liquid-crystal core component is the partially conjugated phenylcyclohexane. Here the saturated

cyclohexane ring prevent electron delocalization over the entire molecule, thus the torsional potential is governed by steric repulsion of the hydrogens. A previous study has shown that the addition of a polar end group has little effect on the torsional potential [45]. Both the *ab initio* and fitted potentials for phenylcyclohexane are shown in Fig. 5. The fitted potential closely matches the *ab initio*, with a barrier height of 0.120 eV in the *ab initio* potential and 0.116 eV in the fitted potential. These are in good agreement with the experimental value of 0.124 eV [55] found by NMR spectroscopy in the liquid phase.

Moving to nonconjugated systems, we show the torsional potential for butane in Fig. 6. Again a good agreement can be seen between the *ab initio* data and the fitted potential. The eclipse ( $0^\circ$ ) barrier height is 0.251 eV and the *trans-gauche* barrier is 0.140 eV. This system has been well studied, both experimentally [56–59] and theoretically [60]. A study by the Tsuzuki *et al.* [60] compared the rotational barriers of butane calculated by various computational methods, finding *trans-gauche* barriers between 0.142 and 0.159 eV and

TABLE VII. Torsional force constants ( $k_{\tau_n}$ ) used in this study ( $\times 10^{-2}$  eV).

Torsion	$k_{\tau_1}$	$k_{\tau_2}$	$k_{\tau_3}$	$k_{\tau_4}$	$k_{\tau_5}$	$k_{\tau_6}$	$k_{\tau_8}$	$k_{\tau_{10}}$	$k_{\tau_{12}}$
$C_A-C_P-C_P-C_A^a$	0.00	7.90	0.00	1.76	0.00	0.54	0.16	0.03	0.01
$C_A-C_P-C_P-C_A^b$	0.00	9.57	0.00	0.11	0.00	0.19	0.25	0.07	-0.04
$C_A(F)-C_P-C_P-C_A$	0.00	4.87	0.00	-1.48	0.00	-0.07	0.00	-0.03	0.05
$C_A-C_A-C_A-C_A$	0.00	41.24	0.00	0.00	0.00	0.00	0.00	0.00	0.00
$C_n-C_n-C_n-C_n$	8.47	0.32	0.12	-1.63	0.17	0.06	0.00	0.00	0.00
$HC-C_n-C_n-C_n$	0.00	0.00	0.16	0.00	0.00	0.00	0.00	0.00	0.00
$HC-C_n-C_n-HC$	0.00	0.00	0.14	0.00	0.00	0.00	0.00	0.00	0.00
$C_A-C_A-H_A-C_A$	0.00	4.34	0.00	0.00	0.00	0.00	0.00	0.00	0.00
$C_A-C_n-C_n-C_n$	3.04	0.03	-0.14	0.55	0.00	0.25	0.00	0.00	0.00
$C_A-C_A-C_n-C_n^c$	0.00	3.59	0.00	-0.29	0.00	-0.21	0.08	0.00	0.00
$C_A-C_A-C_n-C_n^d$	0.00	2.28	0.00	-1.00	0.00	-0.20	0.00	0.00	0.00

<sup>a</sup>Torsional force constants for biphenyl.<sup>b</sup>Torsional force constants for 4-cyanobiphenyl.<sup>c</sup>Torsional force constants for propylbenzene.<sup>d</sup>Torsional force constants for phenylcyclohexane.

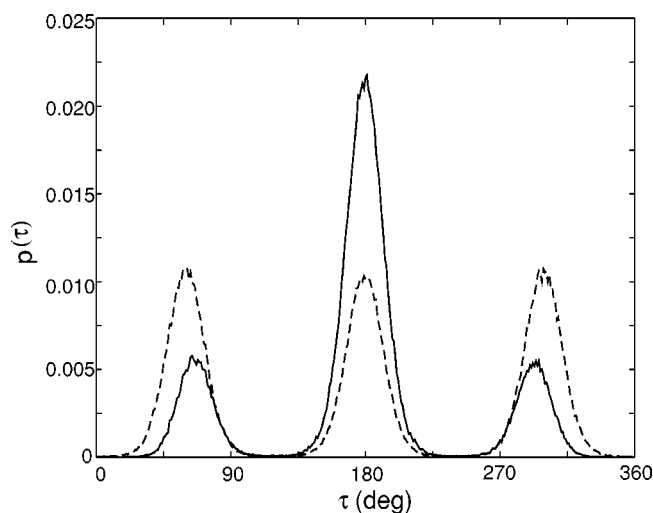


FIG. 7. Liquid phase dihedral angle distributions of butane at 272.5 K, i.e., the C3-C2-C2-C3 dihedral distribution (—) and the HC-C3-C2-C2 dihedral distribution (---).

eclipse barriers between 0.245 and 0.268 eV, to which our results compare favorably. Our values for the *trans-gauche* energy difference (*ab initio* potential 0.034 eV, fitted potential 0.035 eV) are in better agreement with experimental values than those calculated up to the MP2 level and with DFT using a localized basis set. These results are displayed fully in Table VI.

The full set of torsional force constants  $k_m$  is given in Table VII.

### B. Condensed phase molecular dynamics simulations

To test our parametrized force field, we have performed molecular dynamics simulations on several liquid-crystal fragments. The details of the method used have been outlined in Sec. III C. From these we have examined the geometries and thermodynamic properties of the bulk materials including densities and heats of vaporization.

The dihedral angle distribution for butane is shown in Fig. 7. The distribution for the central C-C-C-C dihedral angle has a large central peak at 180° corresponding to the *trans* conformer and two smaller peaks at about 60° and 300° corresponding to the *gauche* conformers, as expected from the *ab initio* potential. Integrating this distribution gives a *trans* population of 67.50% and *gauche* populations of 16.60% and 15.89%, respectively. This compares well with previous simulations of butane, which found a *trans* population of 67.8% [61]. It is also in good agreement with the *trans* population calculated from Raman scattering of 70.7% [57]. Previous studies have shown little change in the *trans* population of butane in going from the gas phase to the liquid phase [61]. The C-C-C-H dihedral angle shows three peaks at 60°, 180°, and 300°, of roughly equal height, which is consistent with the threefold symmetry in its torsional potential. Figure 8 shows the dihedral angle distributions for the C-C-C-C dihedrals in liquid phase hexane and compares them to that of butane. Considering Fig. 8(a) we can see that the distributions for each dihedral angle in hexane are similar

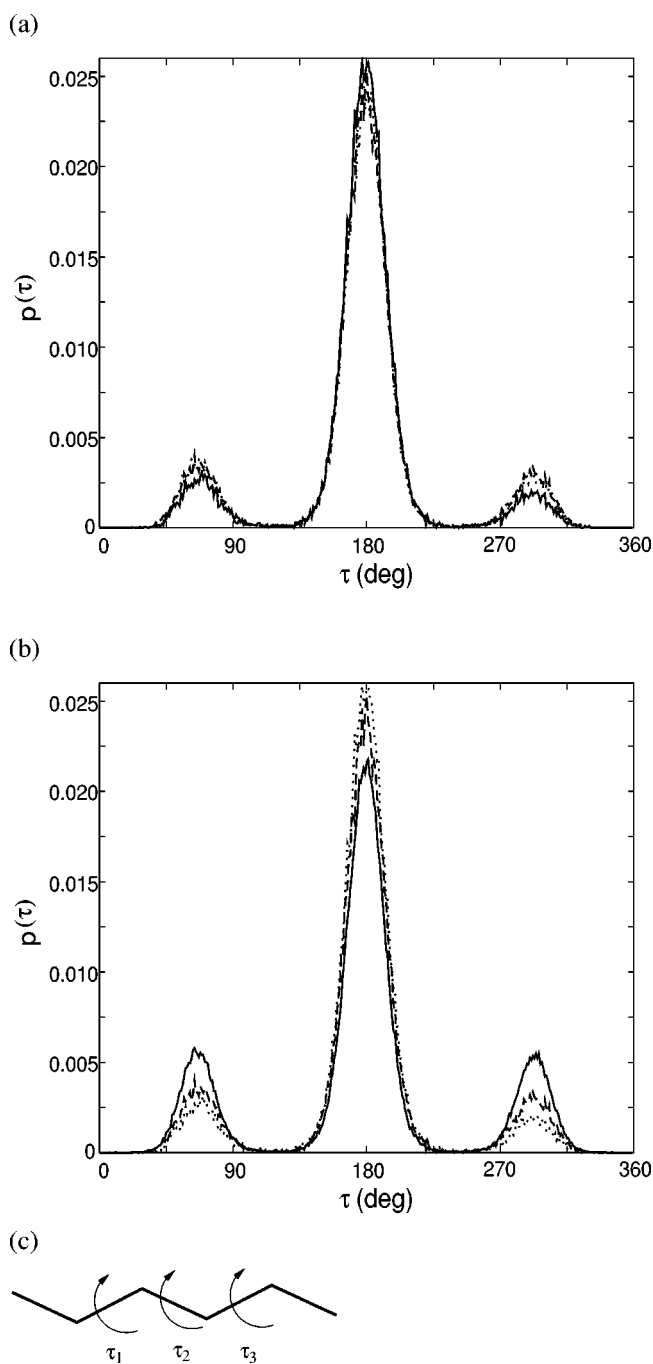


FIG. 8. (a) Liquid phase dihedral angle distributions for hexane at 298 K [dihedral angles  $\tau_1$  ( $\cdots$ ),  $\tau_2$  (—), and  $\tau_3$  (---)]. (b) Liquid phase dihedral angle distributions for butane (—) at 272.5 K and hexane at 298 K [ $\cdots$ ] distribution for angle  $\tau_1$  in hexane, and (—) for angle  $\tau_2$  in hexane]. (c) Structure of hexane with definitions of angles  $\tau_1$ ,  $\tau_2$ , and  $\tau_3$ .

to that of butane, with the central dihedral,  $\tau_2$ , having a larger *trans* population than the outer dihedrals. This is consistent with previous simulation results [62]. From the direct comparison in Fig. 8(b) it can be seen that the *trans* populations for hexane are larger than that of butane.

The dihedral distribution functions for biphenyl and 4-cyanobiphenyl are shown in Fig. 9. In both cases peaks in

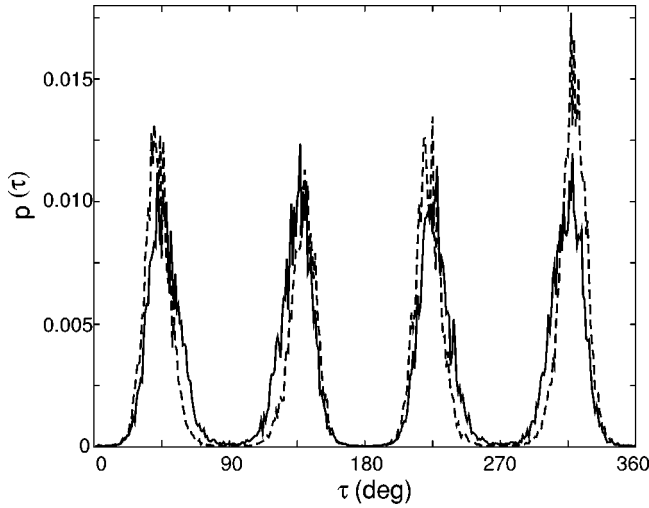


FIG. 9. Liquid phase dihedral angle distributions for biphenyl (—) at 343 K and 4-cyanobiphenyl (---) at 360 K.

the dihedral angle distribution occur at minima in both the fitted and *ab initio* potentials in Fig. 2, and so we notice no significant influence on these from surrounding molecules in the bulk.

The simulation data was used to calculate bulk thermodynamic properties for the sample mesogenic fragments. Densities were calculated from the average system volume, with results shown in Table VIII. As can be seen, there is good agreement between the experimental values [34,63] and those obtained from simulation. This indicates that the terms describing the intermolecular interactions provide a good representation of those in the real fluid.

Following Jorgensen [34], we find the molar heat of vaporization,  $\Delta_{vap}H$  from

$$\Delta_{vap}H = H(g) - H(l), \quad (9)$$

where  $H = E_{inter} + E_{intra} + pV$  and  $l$  and  $g$  indicate liquid and gas phase values, respectively. For a liquid at ambient pressure the  $pV$  term is negligible [ $V(l)$  is about  $0.001V(g)$ ], while due to the very weak intermolecular interactions in the gas phase we can assume ideality; thus  $E_{inter}(g)$  is zero and  $pV = RT$ . Therefore,

$$\Delta_{vap}H = E_{intra}(l) - [E_{intra}(l) + E_{inter}(l)] + RT. \quad (10)$$

TABLE VIII. Computed and experimental densities of sample liquids.

Liquid	$T$ (K)	$\langle V \rangle$ ( $\text{\AA}^{-3}$ )	$\langle \rho \rangle$ ( $\text{kg m}^{-3}$ )	$\langle \rho \rangle$ (expt) ( $\text{kg m}^{-3}$ )	References	Error (%)
Biphenyl	343	56373	$981.3 \pm 7.1$	990	[63]	1.0
4-Cyanobiphenyl	360	62485	$1028.7 \pm 6.8$			
Butane	272.5	34685	$605.3 \pm 10.6$	602	[34]	0.5
<i>n</i> -Propylbenzene	298	50388	$861.8 \pm 7.8$	860	[64]	0.2
Phenylcyclohexane	298	60620	954.9	939	[64]	1.7
2-Fluorobiphenyl	343	57303	1085.6			
Hexane	298	46860	$664.3 \pm 8.0$	656	[64]	1.3
Terphenyl	493	89217	$932.4 \pm 8.8$	957.7	[64]	2.6

Calculated values of the  $\Delta_{vap}H$  are listed in Table IX along with the experimental values [64]. Where available, these are in good agreement with the calculated values. The heat of vaporization depends critically on the average molecular structure as governed by the intramolecular potentials, in addition to the intermolecular potential, so the agreement with experiment is encouraging.

Diffusion coefficients have been calculated for the sample molecules using the Einstein relationship [65]

$$D = \frac{1}{6t} \langle |\mathbf{r}_i(t) - \mathbf{r}_i(0)|^2 \rangle, \quad (11)$$

where  $\mathbf{r}_i$  is the position of the center of mass of a particular atom. The values for the diffusion coefficients for the sample molecules are shown in Table X. The diffusion coefficient for butane was calculated by Davis and Evans to be  $7.4 \times 10^{-9} \text{ m}^2 \text{ s}^{-1}$  using equilibrium molecular dynamics [66]. This was, however, calculated at a lower system density ( $583 \text{ kg m}^{-3}$ ) and extrapolated to infinite system size, both factors strongly influencing the diffusion.

The center of mass radial distribution functions for butane and hexane are shown in Fig. 10(a). The radial distribution function (rdf) for butane is typical for a fluid near a phase transition [65] (this simulation was conducted at the boiling point of butane), with a broad first solvation peak at about  $5.4 \text{ \AA}$ . For hexane the rdf shows a broad peak starting at about  $5.3 \text{ \AA}$  and peaking at about  $6.9 \text{ \AA}$ . The center of mass radial distribution functions for biphenyl, 4-cyanobiphenyl, and 2-fluorobiphenyl are shown in Fig. 10(b). Again they have the expected form, with the onset of first solvation peaks for biphenyl and 2-fluorobiphenyl at about  $4 \text{ \AA}$  with the peak centered around  $7.5 \text{ \AA}$ , and the onset of first solvation peak for 4-cyanobiphenyl at about  $3.5 \text{ \AA}$  with the peak centered at about  $5 \text{ \AA}$ . The similarity in the radial distribution functions for biphenyl and 2-fluorobiphenyl is expected due to their similar molecular shapes. The first peak in 4-cyanobiphenyl is closer than in the other biphenyls due to closer molecular packing caused by strong dipole-dipole interactions between molecules.

## V. CONCLUSION

In this paper we have presented a methodology for generating force field parameters from high level density functional calculations, and have applied it to the generation of a

TABLE IX. Computed and experimental heats of vaporization for sample liquids. All energies in  $\text{kJ mol}^{-1}$ .

Liquid	$T$ (K)	$E_{intra} + E_{inter}(l)$	$E_{intra}(g)$	$\Delta_{vap}H$	$\Delta_{vap}H(\text{expt})$	References	Error (%)
Biphenyl	343	-9.669	50.472	62.99	61.23	[64]	2.9
4-Cyanobiphenyl	360	-34.024	43.095	77.119			
Butane	272.5	17.03	36.43	21.67	22.44	[64]	3.4
<i>n</i> -Propylbenzene	298	28.46	71.86	45.88	46.48	[64]	1.3
Phenylcyclohexane	298	19.84	83.77	66.41	64.14	[64]	3.5
2-Fluorobiphenyl	343	62.74	112.82	31.66			
Hexane	298	7.56	38.22	33.13	31.98	[64]	3.6
Terphenyl	493	190.98	123.06	72.02	75.89	[64]	5.1

force field for liquid crystals. We have then tested the force field using molecular dynamics simulations from which key thermodynamic properties have been computed.

The results from this study are very promising. In the simulation, our force field has been able to reproduce experimental densities and heats of vaporization, with errors of about 2% and 3%, respectively. We have also been able to reproduce *ab initio* torsional potentials for a range of torsional potentials. This is important as a good representation of conformational profiles is important for good quality simulations of soft matter.

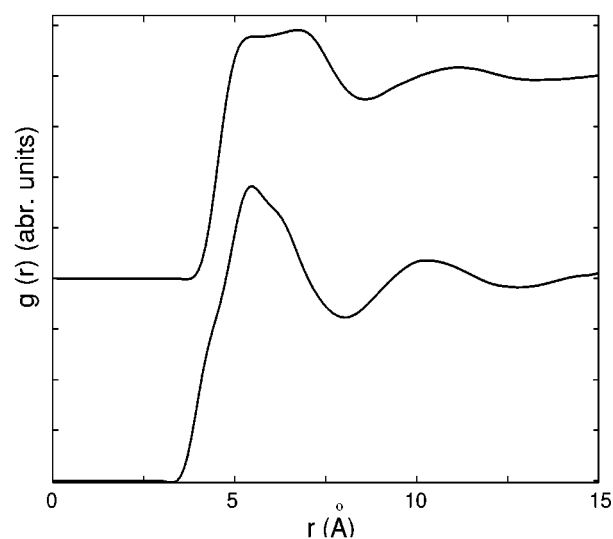
The wide range of molecules that form liquid-crystal phases dictates the need for easy generation of new force field parameters. We have accomplished this by the use of a simple functional form for the force field and the use of accurate, but relatively computationally inexpensive *ab initio* density functional calculations. The use of “off the shelf” values for van der Waals parameters and charges also helps in this regard.

A number of extensions of the current work are possible. One possibility is the investigation of charges derived from the *ab initio* electrostatic potential [67] as well as charges from a Mulliken-like analysis. Charges derived from electrostatic moments have already been used for aromatic carbon and hydrogen atoms and extension to other atom types is possible. The range of the parametrization can also be extended to cover further functional groups common in liquid-crystal molecules, notably linking groups such as esters and further ring-tail groups, which are important in determining the overall shape of liquid-crystal molecules.

TABLE X. Diffusion coefficients.

Liquid	$T$ (K)	$D$ ( $\times 10^{-9} \text{ m}^2 \text{ s}^{-1}$ )
Biphenyl	343	0.718
4-Cyanobiphenyl	360	0.555
Butane	272.5	4.741
<i>n</i> -Propylbenzene	298	1.006
Phenylcyclohexane	298	0.205
2-Fluorobiphenyl	343	0.634
Hexane	298	3.152
Terphenyl	493	1.939

(a)



(b)

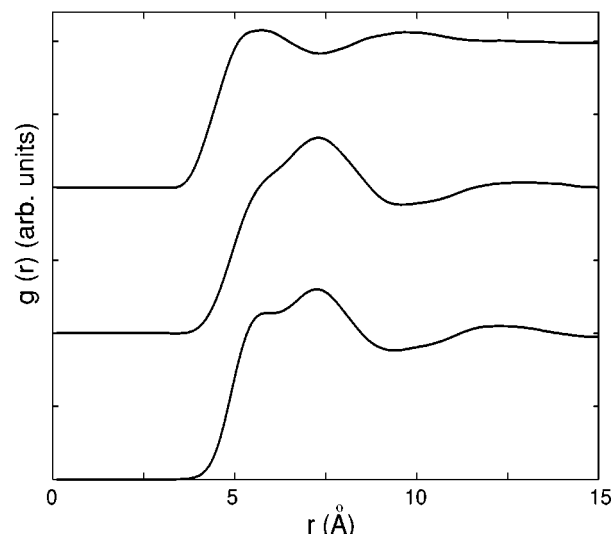


FIG. 10. (a) Radial distribution functions for liquid butane at 272.5 K and liquid hexane at 298 K. (b) Radial distribution functions for liquid biphenyl at 343 K, liquid 2-fluorobiphenyl at 343 K, and liquid 4-cyanobiphenyl at 360 K. In both graphs, successive curves are offset 1 unit along the y axis.

Finally, recent studies in our laboratory have shown that it is now possible to study systems of up to 1000 mesogens in the isotropic phase [68] using parallel molecular dynamics methods on multiprocessor machines. Work is currently underway to test the force field developed in this work for similar system sizes in a liquid-crystal phase. Such studies

open the way for the prediction of key material properties important in liquid-crystal displays.

#### ACKNOWLEDGMENT

One of us (D.L.C.) would like to thank the UK EPSRC for financial support.

- 
- [1] D. Frenkel, B.M. Mulder, and J.P. McTague, *Phys. Rev. Lett.* **52**, 287 (1984).
- [2] J.A.C. Veerman and D. Frenkel, *Phys. Rev. A* **41**, 3237 (1990).
- [3] J.G. Gay and B.J. Berne, *J. Chem. Phys.* **74**, 3316 (1981).
- [4] E. de Miguel, L.F. Rull, M.K. Chalam, and K.E. Gubins, *Mol. Phys.* **74**, 405 (1991).
- [5] G.R. Luckhurst, R.A. Stephans, and R.W. Phippen, *Liq. Cryst.* **8**, 451 (1990).
- [6] R. Beradi, A.P. Emerson, and C. Zannoni, *J. Chem. Soc., Faraday Trans.* **89**, 4069 (1993).
- [7] M.R. Wilson, *Mol. Phys.* **81**, 675 (1993).
- [8] D.A. Dunmur, M. Grayson, B.T. Pickup, and M.R. Wilson, *Mol. Phys.* **90**, 179 (1997).
- [9] M.R. Wilson, in *Advances in the Computer Simulations of Liquid Crystals*, edited by P. Pasini and C. Zannoni (Kluwer Academic, Dordrecht, The Netherlands, 2000).
- [10] M.R. Wilson and M.P. Allen, *Mol. Cryst. Liq. Cryst.* **198**, 389 (1991).
- [11] M.R. Wilson and M.P. Allen, *Liq. Cryst.* **12**, 157 (1992).
- [12] A.V. Komolkin, A. Laaksonen, and A. Maliniak, *J. Chem. Phys.* **101**, 4103 (1994).
- [13] C.W. Cross and B.M. Fung, *J. Chem. Phys.* **101**, 6839 (1994).
- [14] M.A. Glaser, R. Malzbender, N.A. Clark, and D.M. Walba, *J. Phys.: Condens. Matter* **6**, 261 (1994).
- [15] S. Hauptmann, T. Mosell, S. Reiling, and J. Brickmann, *Chem. Phys.* **208**, 57 (1995).
- [16] S.Y. Yakovenko, A.A. Muravski, F. Eikelschulte, and A. Geiger, *J. Chem. Phys.* **105**, 10766 (1996).
- [17] C. McBride, M.R. Wilson, and J.A.K. Howard, *Mol. Phys.* **93**, 955 (1998).
- [18] K.-J. Lee, G.-H. Hsuie, J.-L. Wu, and J.-H. Chen, *Liq. Cryst.* **26**, 46 (1999).
- [19] W.D. Cornell, P. Cieplak, C.I. Bayly, I.R. Gould, K.M. Merz, D.M. Ferguson, D.C. Spellmeyer, T. Fox, J.W. Caldwell, and P.A. Kollman, *J. Am. Chem. Soc.* **117**, 5179 (1995).
- [20] N. Allinger, K. Chen, and J.-H. Lii, *J. Comput. Chem.* **17**, 642 (1996).
- [21] N. Nevins, K. Chen, and N. Allinger, *J. Comput. Chem.* **17**, 669 (1996).
- [22] N. Nevins, J.-H. Lii, and N. Allinger, *J. Comput. Chem.* **17**, 695 (1996).
- [23] N.L. Allinger, K. Chen, J.A. Katzenellenbogen, S.R. Wilson, and G.M. Anstead, *J. Comput. Chem.* **17**, 747 (1996).
- [24] J.E. Lennard-Jones, *Proc. R. Soc. London, Ser. A* **106**, 463 (1924).
- [25] F. Jensen, *Introduction to Computational Chemistry* (Wiley, Chichester, 1999), Chap. 2.
- [26] P. Hohenberg and W. Kohn, *Phys. Rev.* **B136**, 864 (1964).
- [27] W. Kohn and L.J. Sham, *Phys. Rev.* **A140**, 1133 (1965).
- [28] CASTEP version 3.9, Academic Version, licensed under the UKCP-MSI Agreement, 1999.
- [29] M.C. Payne, M.P. Teter, D.C. Allan, J.D. Joannopolous, and T.A. Arias, *Rev. Mod. Phys.* **64**, 1045 (1992).
- [30] D. Vanderbilt, *Phys. Rev. B* **41**, 7892 (1990).
- [31] J.P. Perdew, J.A. Chevary, S.H. Vosko, K.A. Jackson, M.R. Pederson, D.J. Singh, and C. Fiolhais, *Phys. Rev. B* **46**, 6671 (1992).
- [32] Cerius<sup>2</sup> is a molecular modeling package distributed by Biosym Molecular Simulations Inc., 1999.
- [33] R.P. Feynman, *Phys. Rev.* **56**, 340 (1939).
- [34] W.L. Jorgensen, D.S. Maxwell, and J. Tirado-Rives, *J. Am. Chem. Soc.* **118**, 11225 (1996).
- [35] W.L. Jorgensen, D.S. Maxwell, and J. Tirado-Rives, Support Material for OPLS-AA Force Field (unpublished).
- [36] W.L. Jorgensen and T.B. Nguyen, *J. Comput. Chem.* **14**, 195 (1993).
- [37] W.H. Press, B.P. Flannery, S.A. Teukolsky, and W.T. Vetterling, *Numerical Recipes* (Cambridge University Press, Cambridge, England, 1992), Chap. 10.
- [38] W. Smith and T.R. Forester, computer code DL-POLY copyright The Council for the Central Laboratory of the Research Councils (Daresbury Laboratory, Daresbury, Nr. Warrington, 1996).
- [39] J.P. Ryckaert, G. Ciccotti, and H.J.C. Berendsen, *J. Comput. Phys.* **23**, 327 (1977).
- [40] S. Nosé, *J. Chem. Phys.* **53**, 255 (1984).
- [41] M.P. Allen and D.J. Tildesley, *Computer Simulation of Liquids* (Clarendon Press, Oxford, 1989), Chap. 5.
- [42] M.J. Cook and M.R. Wilson, *Mol. Cryst. Liq. Cryst. Sci. Technol., Sect. A* **357**, 149 (2001).
- [43] N.L. Allinger, Y.H. Yuh, and J.H. Lii, *J. Am. Chem. Soc.* **111**, 8511 (1989).
- [44] T.A. Halgren, *J. Comput. Chem.* **17**, 616 (1996).
- [45] C.J. Adam, S.J. Clark, M.R. Wilson, G.J. Ackland, and J. Crain, *Mol. Phys.* **93**, 947 (1998).
- [46] S. Tsuzuki, T. Uchimaru, K. Matsumura, M. Mikami, and K. Tanabe, *J. Chem. Phys.* **110**, 2858 (1999).
- [47] A. Karpfen, C.H. Choi, and M. Kertesz, *J. Phys. Chem. A* **101**, 7426 (1997).
- [48] S. Arulmozharaja and T. Fujii, *J. Chem. Phys.* **115**, 10589 (2001).
- [49] A. Almendinger, O. Bastiansen, L. Fernholt, B.N. Cyvin, S.J. Cyvin, and S. Samdal, *J. Mol. Struct.* **128**, 59 (1985).
- [50] O. Bastiansen and S. Samdal, *J. Mol. Struct.* **128**, 115 (1985).
- [51] L.A. Carreira and T.G. Towns, *J. Mol. Struct.* **41**, 1 (1977).
- [52] G. Celebre, G. de Luca, M. Longeri, C. Veracini, and J.W. Emsley, *J. Chem. Soc., Faraday Trans.* **87**, 2623 (1991).
- [53] D.J. Cleaver and D.J. Tildesley, *Mol. Phys.* **81**, 781 (1994).

- [54] J.W. Emsley, T.J. Horne, G. Celebre, G. de Luca, and M. Longeri, *J. Chem. Soc., Faraday Trans.* **88**, 1679 (1992).
- [55] E.L. Eliel and M. Manoharan, *J. Org. Chem.* **46**, 1959 (1981).
- [56] K.S. Pitzer, *J. Chem. Phys.* **8**, 711 (1940).
- [57] D.A.C. Compton, S. Montero, and W.F. Murphy, *J. Phys. Chem.* **84**, 3587 (1980).
- [58] M. Rasanen and V.E. Bondybey, *J. Chem. Phys.* **82**, 4718 (1985).
- [59] R.K. Heenan and L.S. Bartell, *J. Chem. Phys.* **78**, 1270 (1983).
- [60] S. Tsuzuki, T. Uchimaru, and K. Tanabe, *Chem. Phys. Lett.* **246**, 9 (1995).
- [61] W.L. Jorgensen, *J. Am. Chem. Soc.* **103**, 4721 (1981).
- [62] W.L. Jorgensen, J.D. Madura, and C.J. Swenson, *J. Am. Chem. Soc.* **106**, 6638 (1984).
- [63] P.A. Irvine, D.C. Wu, and P.J. Flory, *J. Chem. Soc., Faraday Trans. 1* **80**, 1795 (1984).
- [64] C.L. Yaws, *Chemical Properties Handbook* (McGraw-Hill, New York, 1999).
- [65] M.P. Allen and D.J. Tildesley, *Computer Simulation of Liquids* (Clarendon Press, Oxford, 1989), Chap. 2.
- [66] P.J. Davis and D.J. Evans, *J. Chem. Phys.* **103**, 4261 (1995).
- [67] E. Sigfridsson and U. Ryde, *J. Comput. Chem.* **19**, 377 (1998).
- [68] M.J. Cook and M.R. Wilson, *Mol. Cryst. Liq. Cryst. Sci. Technol., Sect. A* **363**, 181 (2001).